

An AUV Survey in the Littoral Zone: Small-Scale Subsurface Variability Accompanying Synoptic

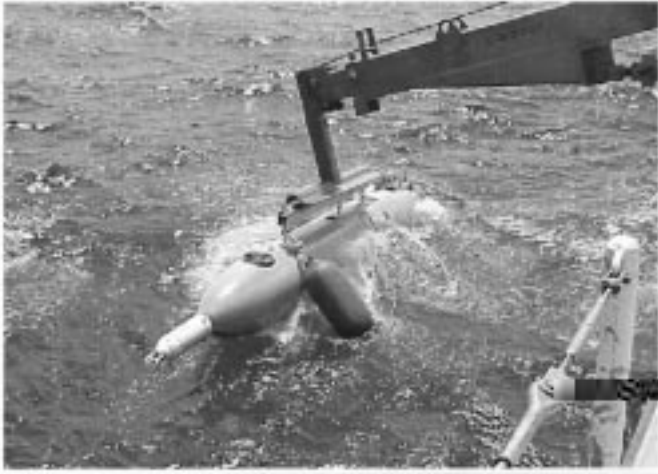


Fig. 1. The OEX AUV. The turbulence package and the upward-looking ADCP are visible in the picture.

potential of an element of such a network. The total network would potentially provide a much larger spatial coverage and/or at a faster rate and represent a powerful subsurface capability that would compliment synoptic remotely sensed observations in support of real-time oceanography. A number of other independent efforts toward the application of AUVs as reliable mobile platforms for oceanographic instruments have been undertaken in the U.S. and Europe [7]–[16].

In the work of An *et al.* [10] and Dhanak and Holappa [9], development efforts in application of Florida Atlantic University's Ocean Explorer (OEX) AUV as a platform for oceanographic measurements were described. The 12-h shallow-water AUV survey described here is an extension of these earlier efforts. The shallow-water region surveyed lies between two long-shore coral reefs and is subject to very complex flows involving interaction between horizontal shear layers along the edge of the

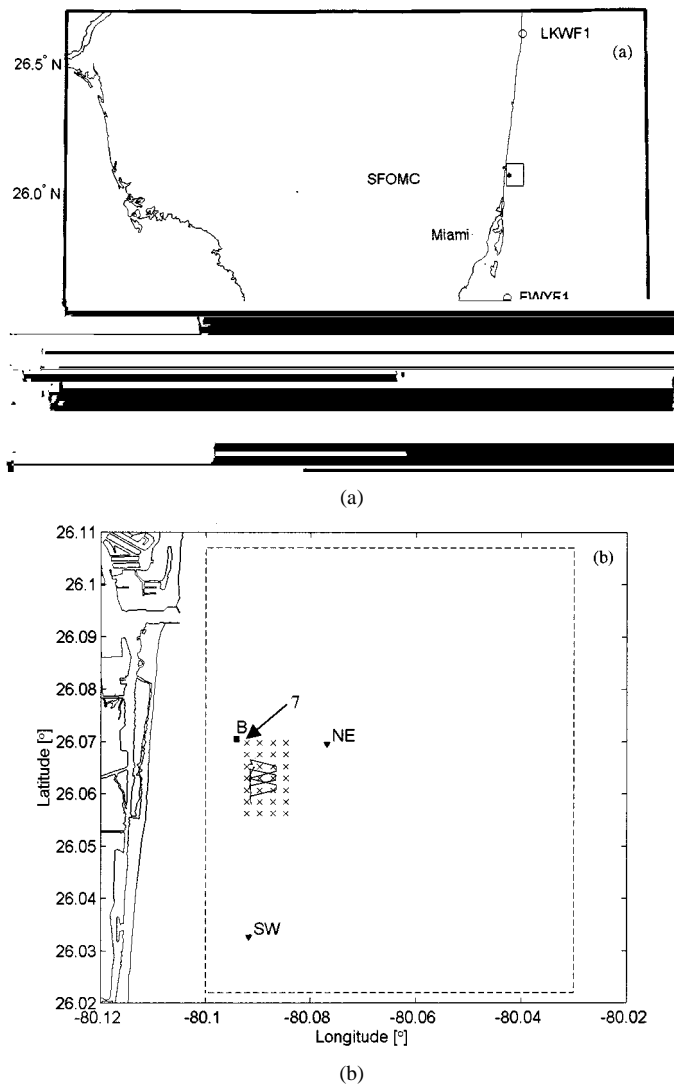


Fig. 2. (a) Site location off the east coast of Florida. The rectangle marks the OSKR observational field and the shaded area within marks the AUV survey region. (b) Close-up map of the survey region. The dashed rectangle approximately denotes the OSKR coverage region and some of the grid points are shown as "x." The AUV path over the grid points is depicted in the figure.

on-board computer, including instantaneous vehicle position in latitude and longitude, vehicle depth and altitude, current profiles at the vehicle location, and *in situ* conductivity and temperature. The turbulence package separately stored the microstructure data, acquired at 450 Hz.

B. OSKR and Ship-Based Sensor Measurements

The dual-frequency OSKR of the University of Miami, described in detail by Haus *et al.* [1], can use HF (25.4 MHz) and VHF (49.9 MHz) radio frequencies to map surface current patterns over a large area in coastal waters. The shore-based radar system consists of two units (master and slave) deployed sev-

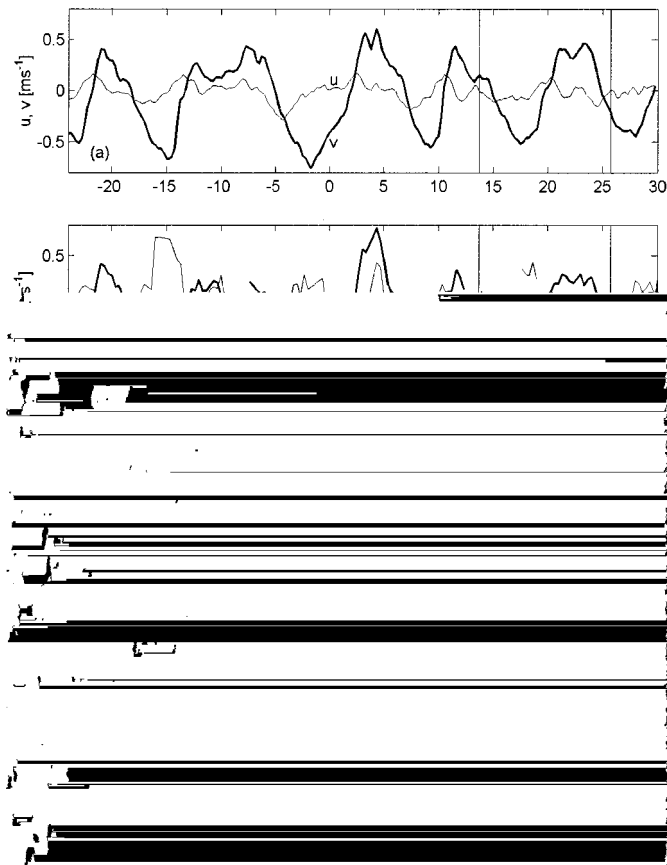


Fig. 4. Time Series of east (u) and north (v) components of: (a) subsurface current at 2.5-m depth recorded at the ADCP B, and (b) of surface current at OSCR grid point 7, (c) winds, and (d) air pressure recorded at the NE buoy. The vertical lines mark the start and end times of the AUV survey.

14 to 21 m. The OSCR coverage, in VHF mode, spanned an approximately 6×12 km region around the AUV survey box. The Florida current flows east of this region, bearing significant influence on the littoral waters [19]. In particular, the periodic cross-shelf meanders of the Florida current strongly influence the strength of the local currents. Further, eddies shed off the Florida current sometimes slowly propagate along the edge of the current [18]. In addition, the coastal region is influenced by periodic discharge of fresher water from local inlets. During the experiment, the local thermocline was located at around 10–15-m water depth. The characteristics of the mi-
 n-

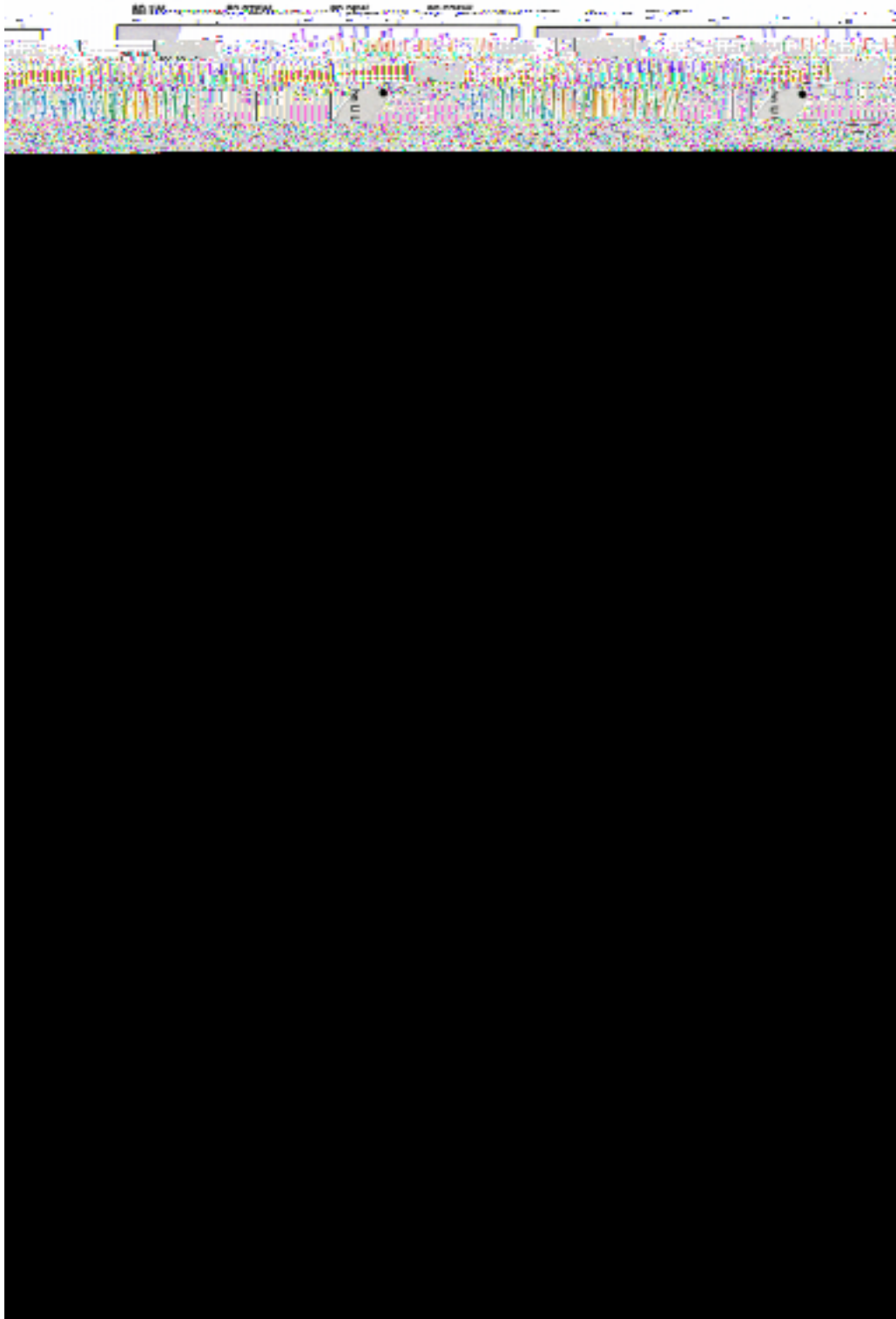


Fig. 7 Nine representative synoptic views of the surface current field over the 12-h period as measured by the OSCR. The velocity vectors are color coded for magnitude. The black box marks the region surveyed by a surface ship and the red box marks the region surveyed by the AUV.

three different depths. The variability of the depth of the thermocline is evident from the figures. It varies from 10 m to beyond 15 m, the mean temperature gradient over the period of the AUV survey being approximately $-0.1 \text{ }^{\circ}\text{C}\cdot\text{m}^{-1}$ in the 5–10 m-depth range, and $-0.2 \text{ }^{\circ}\text{C}\cdot\text{m}^{-1}$ in the 10–15 m-depth range. The time series shown are consistent with corresponding series recorded at the SW buoy, including in

the significant dip in salinity seen around 22 h in the 15-m record. The stratification may be characterized by the 2.5-h time-averaged square buoyancy frequency N^2 [Fig. 3(d)], which has mean values of 0.0017, 0.0012, and 0.0024 s^{-2} at depths 5, 10, and 15 m, respectively. Maximum values occurred at around 1650 GMT. The variation in N^2 at the SW buoy is very similar to that at the NE buoy.

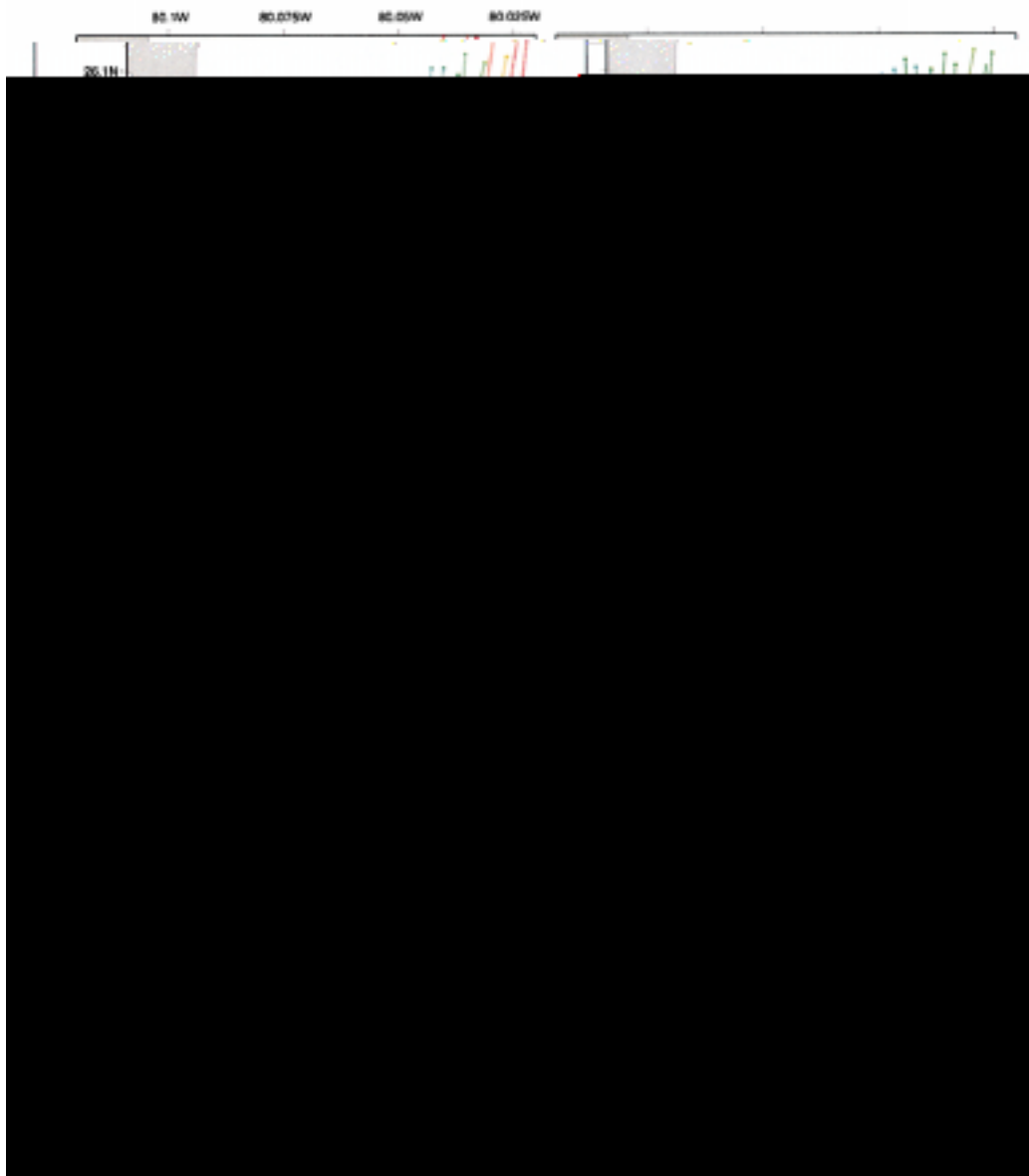


Fig. 7. (*Continued.*) Nine representative synoptic views of the surface current field over the 12-h period as measured by the OSCAR. The velocity vectors are color coded for magnitude. The black box marks the region surveyed by a surface ship and the red box marks the region surveyed by the AUV.

The associated time series of the current at 2.5-m depth, recorded at ADCP B, the corresponding surface current at the OSCAR grid point closest to B [see Fig. 2(b)], referred to below as grid point 7, the prevailing winds at the NE buoy, and the air pressure are shown in Fig. 4. Both the subsurface [Fig. 4(a)] and surface [Fig. 4(b)] time series clearly show substantial oscillations in both the east–west (cross-shelf)

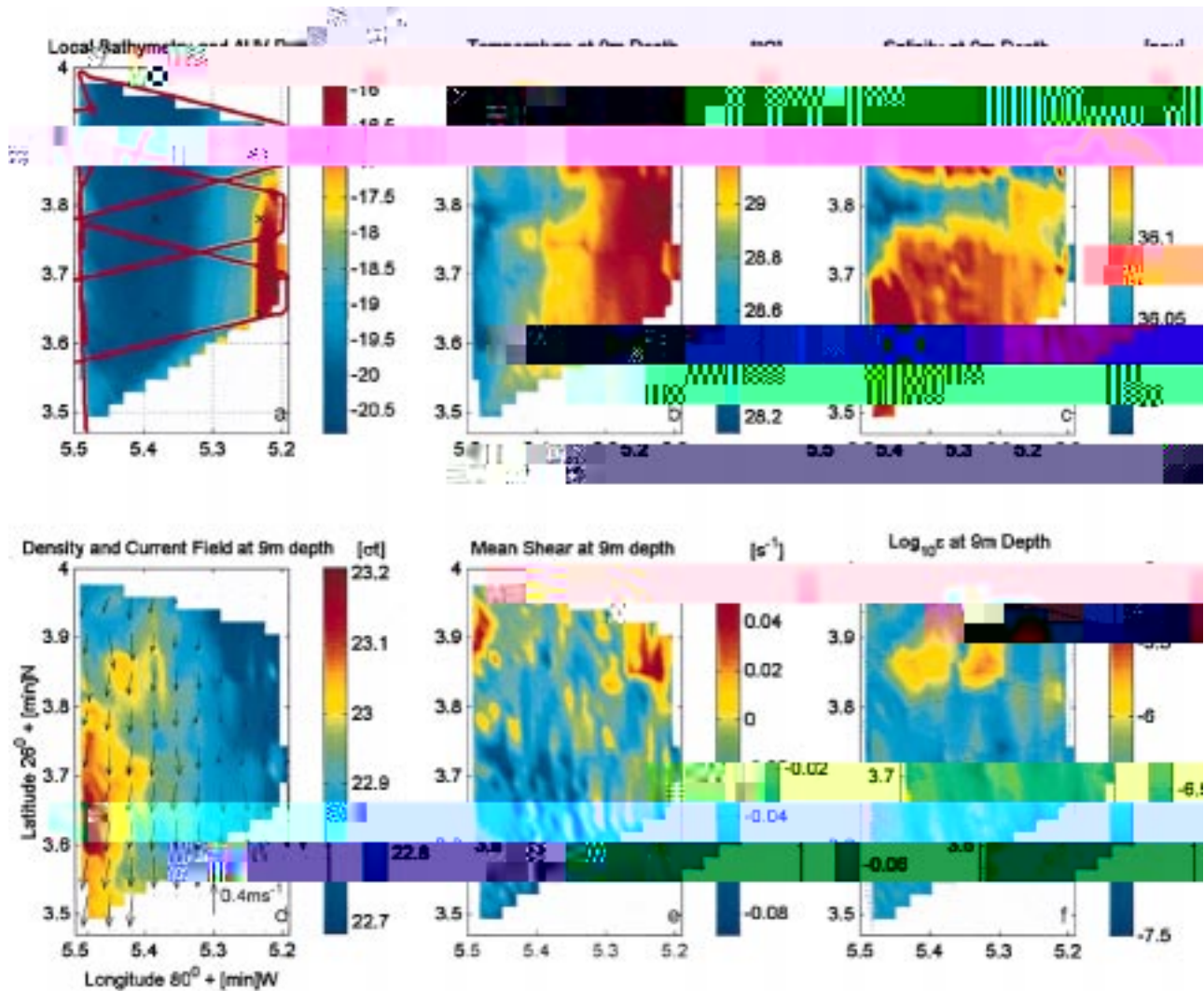


Fig. 8. (a)–(f) Observations from the second segment of the continuous 12-hour AUV survey off the coast of south Florida on 7/27/99. The survey segment shown was carried out during 1524–1646 GMT, giving a nominal mid-range time of 1605 GMT.

box. The winds [Fig. 4(c)] were from the southeast and the speed picked up from $1.5 \text{ m}\cdot\text{s}^{-1}$ at the start of the AUV survey to a maximum of $5.2 \text{ m}\cdot\text{s}^{-1}$ at around 1515 GMT, with a mean speed of $4.2 \text{ m}\cdot\text{s}^{-1}$ over the duration of the 12-h survey. During the survey, the air pressure variation [Fig. 4(d)] did not exceed 2 mbar and 4–5-s-period waves of height not exceeding 0.2 m were recorded at site B.

C. Measurement Survey of July 27, 1999

The 12-hr survey involving AUV-based observations, described here, commenced at 1344 GMT on July 27 and was completed at 0143 GMT on July 28, under monitored background conditions as described above. A general description of all the surveys during July 1999, including a description of the current profile and CTD observations from a surface ship, which moved around the survey box, is given by Shay *et al.* [18]. On July 27, unlike on the other July 1999 surveys, the AUV included sensors for measuring small-scale subsurface turbulence.

1) *OSCR Observations*: The 29-day OSCR observations over the coverage region identified in Fig. 2(b) during July

1999 are described in detail by Shay *et al.* [3] and by Peters *et al.* [4]. Between them, these papers include a comparison of the OSCR observations with the ship-based and NE moored ADCP observations and an analysis of the OSCR field and the ship-based observations. In this section, we briefly describe the OSCR observations on July 27, particularly over the AUV survey box, relating these to the subsurface AUV-based observations.

The OSCR time series at the six grid points, which were located over the AUV coverage area, and at grid point 7 [see Fig. 2(b)], for the period of the AUV survey are shown in Fig. 6(a) and (b). As is apparent, the 10-h oscillation in both u and v was dominant at each of these grid points. Representative

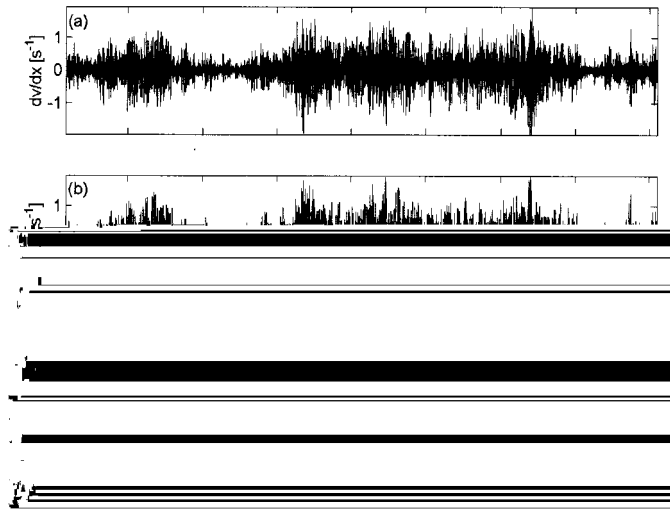


Fig. 10. (a), (b) Two-minute sample microstructure cross-stream shear. (c) Microstructure temperature data.

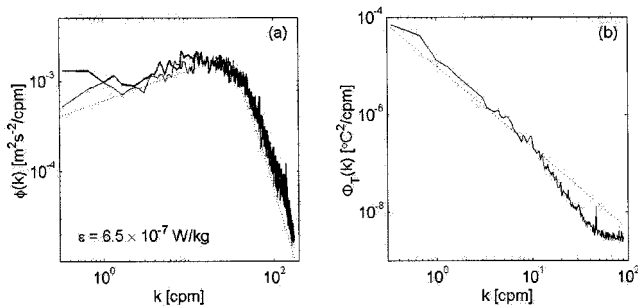


Fig. 11. Spectra of: (a) $\partial v/\partial x$ (thin line) and $\partial w/\partial x$ (thick line) for the time series shown in Fig. 10 (a) and (b), compared with the Nasmyth spectrum (dotted line) and of (b) the temperature time series in Fig. 10(c). The dotted line in (b) indicates $-5/3$ slope.

of the surveyed region is clearly apparent and is consistent with a 1962 U.S. Coast and Geodetic Survey chart.

The recorded water temperature and salinity data from the on-board CTD package for each segment of the survey was used to generate, through interpolation, regional maps of the distribution of temperature, salinity, and water density at 9-m depth for the seven repeated segments of the survey. The maps for the second segment are shown in Fig. 8(b)–(d). It may be noted that these are not synoptic maps; rather, they characterize the spatial distribution of the *in situ* measurements during the mission. Temporal variations on the scale of mission duration or smaller cannot be resolved accurately in such a map. However, temporal variability on a larger scale can be captured from a sequential series of such maps generated from the survey repeated over a significant period. The maps show that, during the period, at 9-m depth, waters in the eastern part of the region are generally warmer and less dense than in the western part of the box. The mean temperature in the box was 29.1

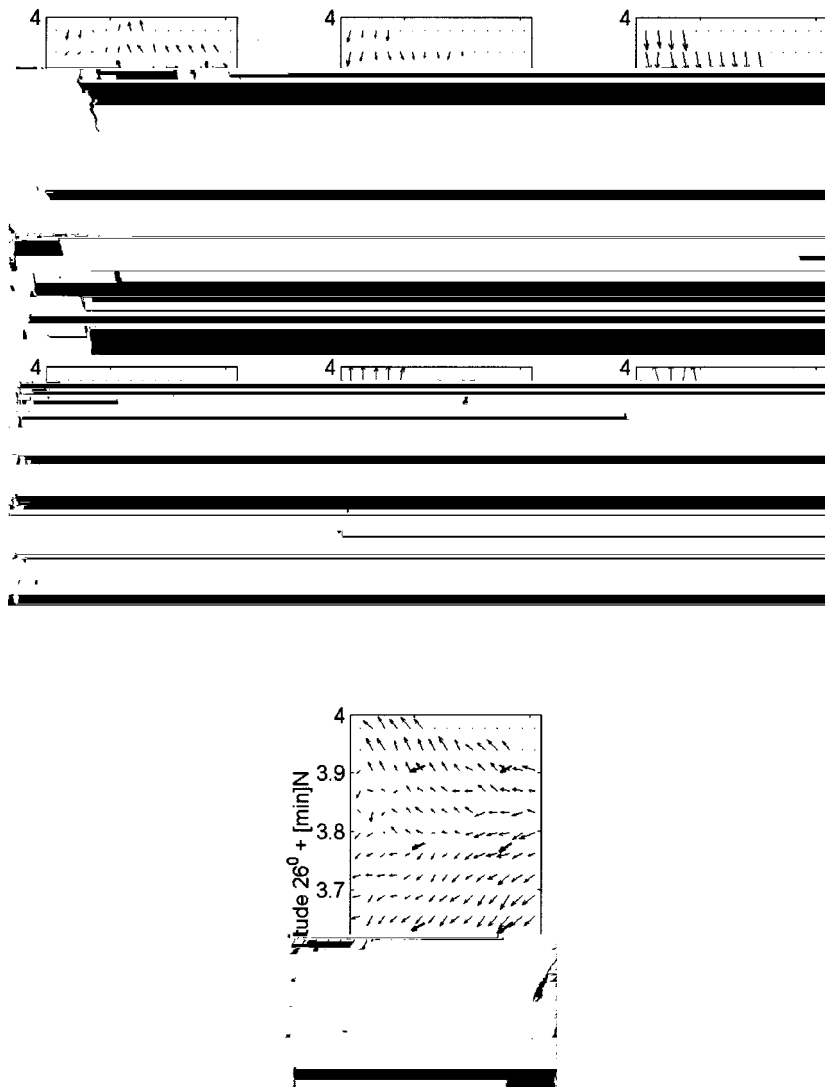


Fig. 14. Maps of the current field at 2.5-m depth as determined from the AUV ADCP measurements and at the surface by OSCR (thicker arrows). The time (GMT) shown in each of the maps (a–g) denote the mid-point of the period of each segment of the survey and approximately correspond to times shown in Fig. 7.

Fig. 9. The figure also shows the corresponding OSCR measurements at the grid points at 1600 GMT. From Fig. 4, a presence of southeasterly winds of around $4 \text{ m}\cdot\text{s}^{-1}$ is evident during the period. As described above, the thermocline during the survey was below 10 m. The vector plots therefore suggest an almost slab-like flow in the mixed layer above the AUV, compared with a rapid clockwise rotation of the velocity vectors below, the magnitude of the velocity decaying with depth, similar to Ekman spirals induced by wind stress.

Sample time series of the microstructure cross-stream shears

$$\partial v / \partial x = 1$$

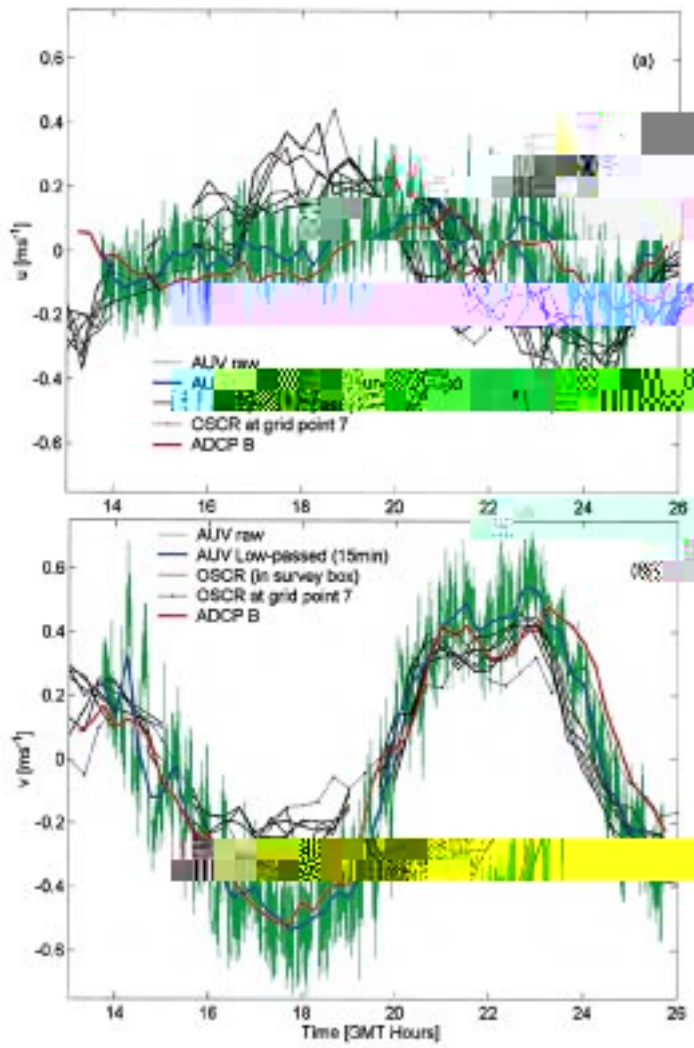
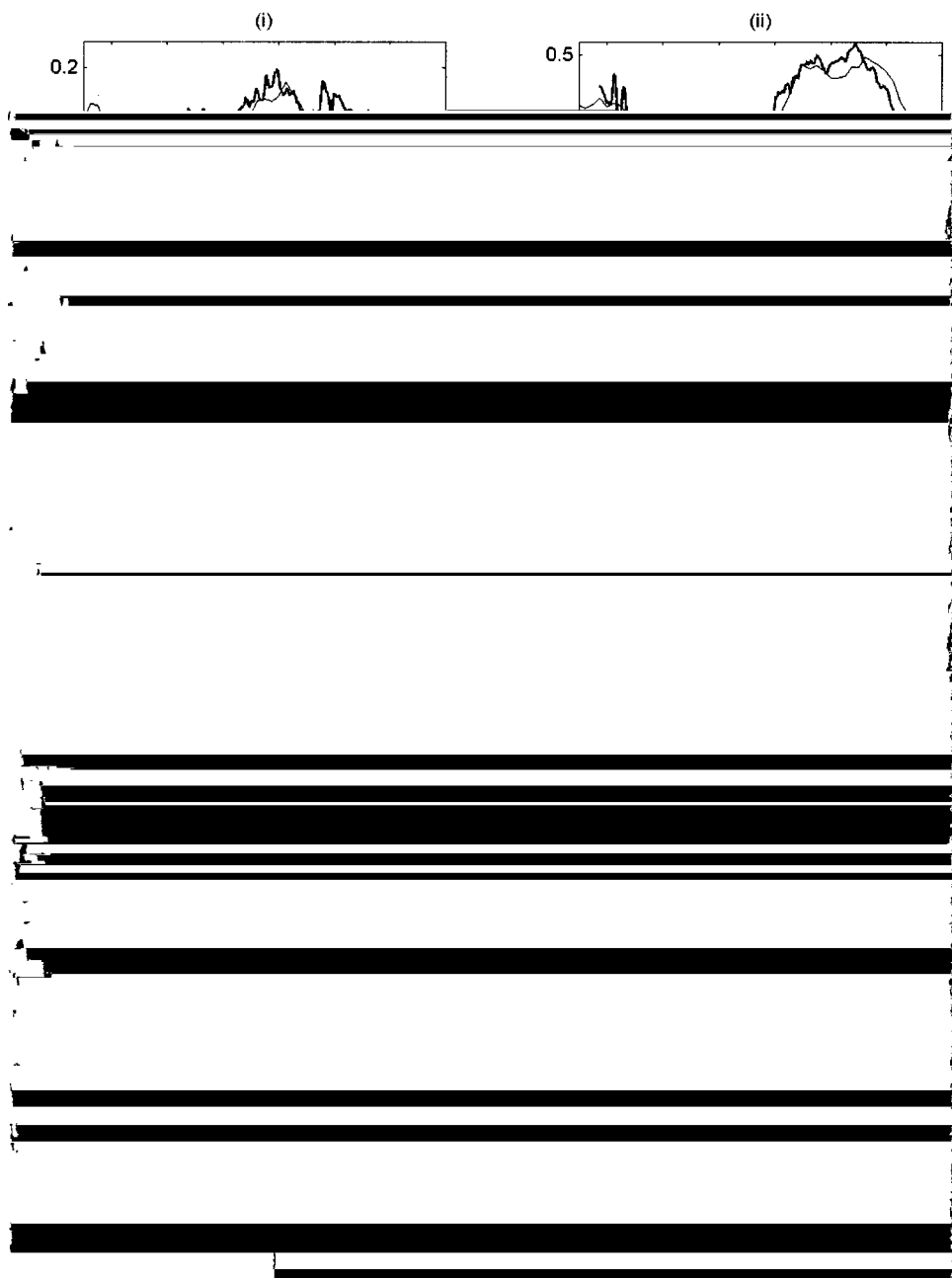


Fig. 15. Time series of: (a) u and (b)



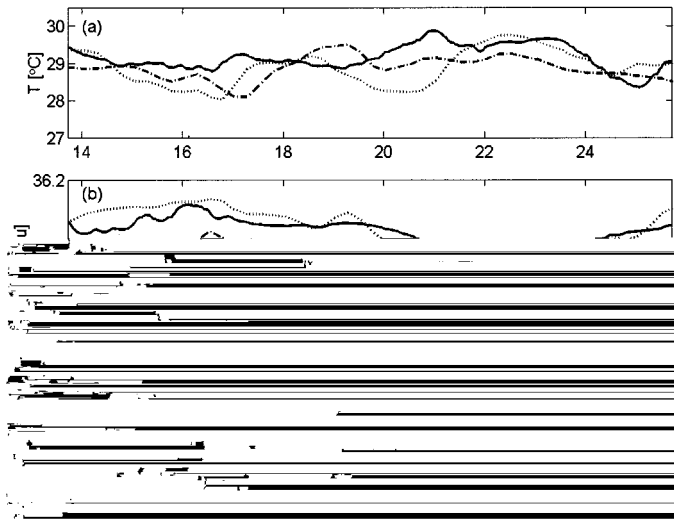


Fig. 17. (a) Temperature, (b) salinity, and (c) density variations during the survey determined from the AUV CT measurements (at 9 m) and the NE and SW USF-Nova CT chain array measurements (at 10 m). AUV conductivity measurements have been adjusted by a constant value of 0.8574 mmho (1.43%) through matching the mean value over the 12-h survey with the mean recorded at the nearby NE CT array.

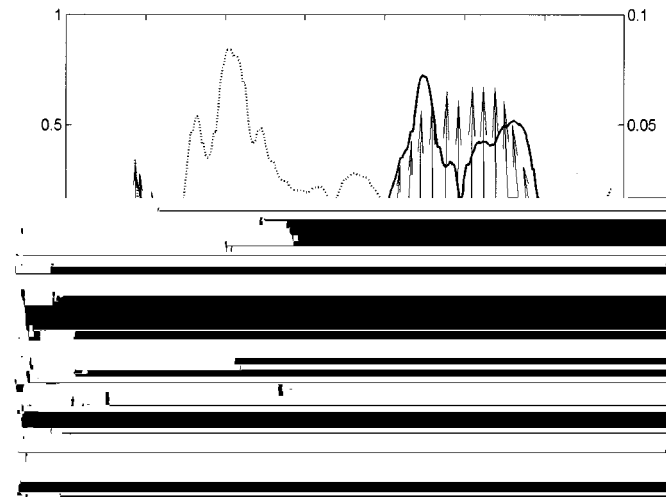


Fig. 18. An overlay of current vector field at 9-m depth, temperature variation ΔT (thick line), and salinity variation Δs , (dotted line) as determined from the AUV measurements. Each time series has been low-pass filtered at 15 min.

for

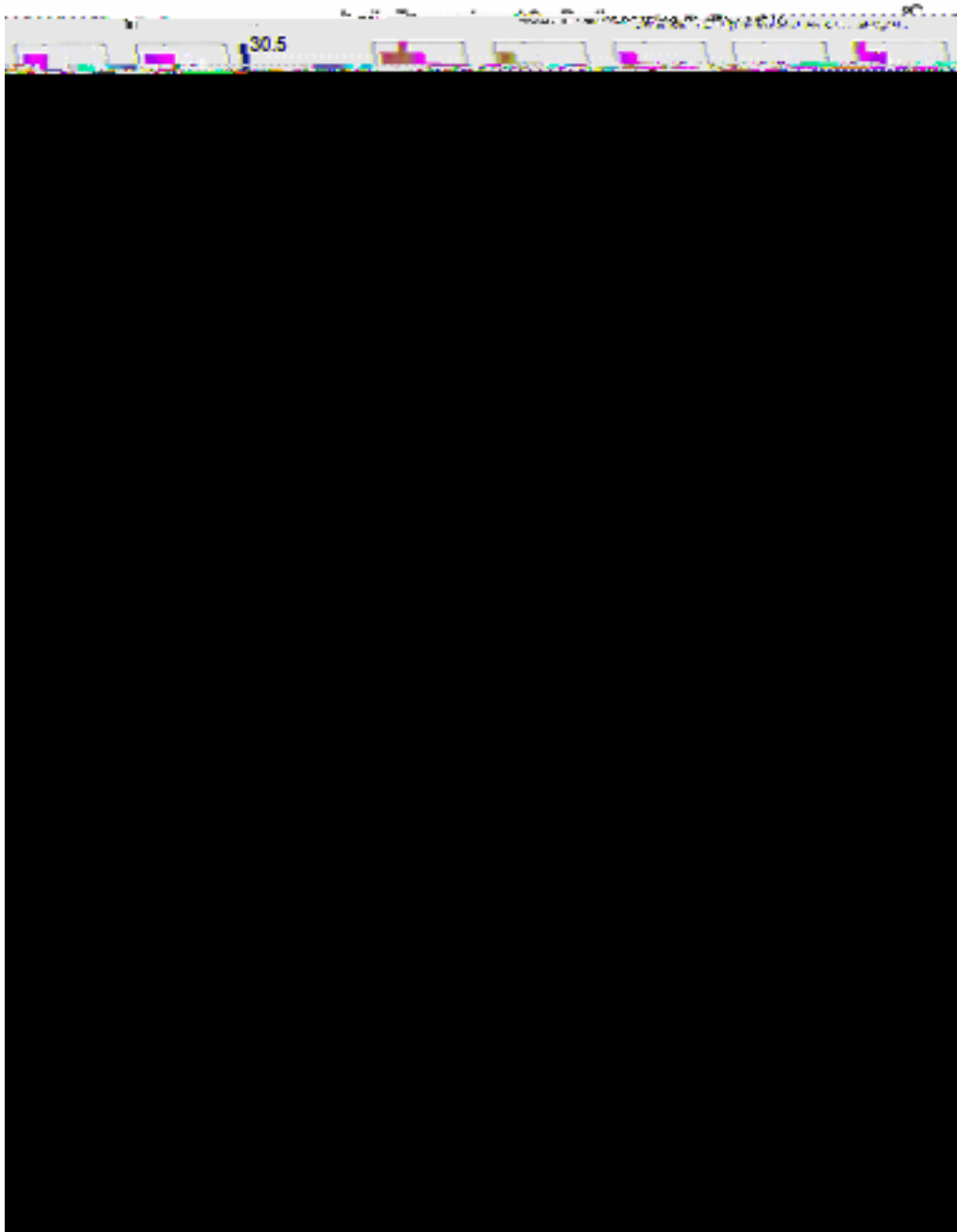


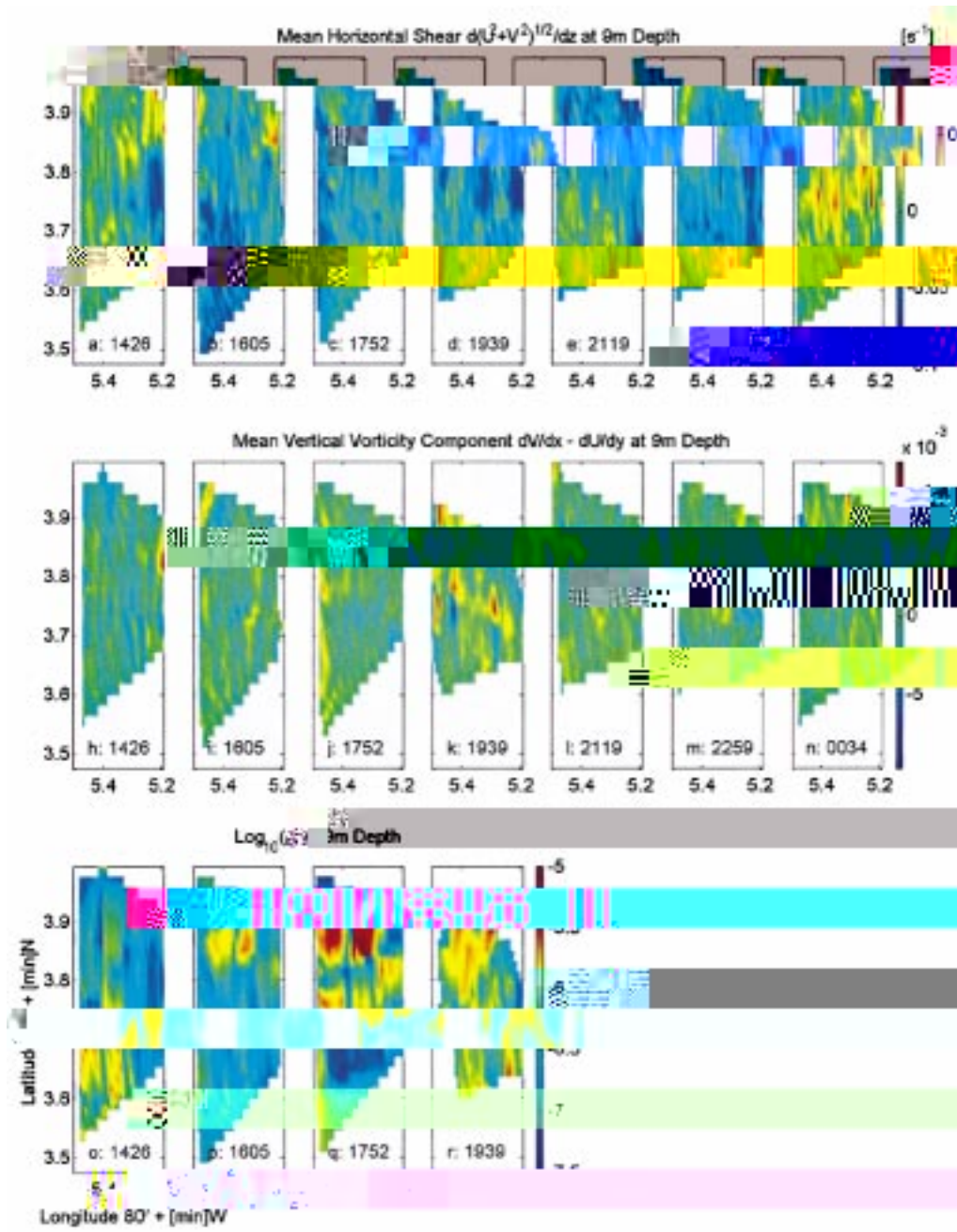
Fig. 20. Maps of the developing temperature (a–g), salinity (h–n), density, and current distributions (o–u) in the survey box at 9-m depth as determined by the AUV observations.

into the survey region from the north during the first half of the current cycle, and were followed by the advection into the AUV survey region of relatively warmer, less saline waters from the south.

5) *Evolution of the Mapped Fields:* The survey maps shown in Fig. 8 were developed for the other segments of the survey to depict the evolution of the mapped fields. These are shown in Figs. 19–21. Fig. 19 shows the 3-D vector maps of the current field beneath the OSCR grid points during the seven segments of the survey. The vertical variation of the vector maps depict the dynamics of the water column: a boundary layer extending over the entire water column when the current was maximum, at approximately 2300 GMT, say (f), and was dominated

by barotropic flow, while featuring rapid turning beneath a slab layer at times of low speeds at approximately 1600, and 2000 GMT, say (b, d), presumably when baroclinic flows dominated.

The evolution of the temperature, salinity, and density maps is shown in Fig. 20. The current fields at the 9-m depth are overlaid in Fig. 20(o)–(u). As described above, temperature variations [Fig. 20(a)–(g)] were generally well correlated with the current, resulting in advection into the region of cooler, more saline waters followed by fresher, warmer waters as the direction of the current shifted. In addition, the waters were generally cooler inshore. However, during segment 4 of the survey, the current was southwards in the east of the region and northwards inshore and resulted in warmer waters inshore and cooler waters offshore.



heat sink in the package and a subsequent 20-h mission, to be reported elsewhere, was successfully conducted during April 2000.

IV. SUMMARY

AUVs as oceanographic measurement platforms, working in conjunction with traditional methods of data acquisition, can be utilized to resolve the flow field over a range of scales. In a rational approach to oceanography, synoptic maps from satellite or HF radar provide larger scale observation of the surface fields. AUV-based surveys of the type described here and measurements from other moored or bottom-mounted instruments complement the synoptic measurements with observations at smaller scales to develop a better understanding of the processes underlying a particular synoptic observation. Developmental efforts have matured sufficiently to make such an approach feasible.

